NASA/CR—2001-210955

# Normal Gravity Testing of a Microchannel Phase Separator for Insitu Resource Utilization

Ward E. TeGrotenhuis and Victoria S. Stenkamp
Battelle Memorial Institute, Richland, Washington

June 2001

The NASA STI Program Office . . . in Profile

Since its founding, NASA has been dedicated to the advancement of aeronautics and space science. The NASA Scientific and Technical Information (STI) Program Office plays a key part in helping NASA maintain this important role.

The NASA STI Program Office is operated by Langley Research Center, the Lead Center for NASA's scientific and technical information. The NASA STI Program Office provides access to the NASA STI Database, the largest collection of aeronautical and space science STI in the world. The Program Office is also NASA's institutional mechanism for disseminating the results of its research and development activities. These results are published by NASA in the NASA STI Report Series, which includes the following report types:

- TECHNICAL PUBLICATION. Reports of completed research or a major significant phase of research that present the results of NASA programs and include extensive data or theoretical analysis. Includes compilations of significant scientific and technical data and information deemed to be of continuing reference value. NASA's counterpart of peer-reviewed formal professional papers but has less stringent limitations on manuscript length and extent of graphic presentations.

- TECHNICAL MEMORANDUM. Scientific and technical findings that are preliminary or of specialized interest, e.g., quick release reports, working papers, and bibliographies that contain minimal annotation. Does not contain extensive analysis.

- CONTRACTOR REPORT. Scientific and technical findings by NASA-sponsored contractors and grantees.

- CONFERENCE PUBLICATION. Collected papers from scientific and technical conferences, symposia, seminars, or other meetings sponsored or cosponsored by NASA.

- SPECIAL PUBLICATION. Scientific, technical, or historical information from NASA programs, projects, and missions, often concerned with subjects having substantial public interest.

- TECHNICAL TRANSLATION. English-language translations of foreign scientific and technical material pertinent to NASA's mission.

Specialized services that complement the STI Program Office's diverse offerings include creating custom thesauri, building customized data bases, organizing and publishing research results . . . even providing videos.

For more information about the NASA STI Program Office, see the following:

- Access the NASA STI Program Home Page at ***http://www.sti.nasa.gov***

- E-mail your question via the Internet to help@sti.nasa.gov

- Fax your question to the NASA Access Help Desk at 301–621–0134

- Telephone the NASA Access Help Desk at 301–621–0390

- Write to:
  NASA Access Help Desk
  NASA Center for AeroSpace Information
  7121 Standard Drive
  Hanover, MD 21076

NASA/CR—2001-210955

# Normal Gravity Testing of a Microchannel Phase Separator for Insitu Resource Utilization

Ward E. TeGrotenhuis and Victoria S. Stenkamp
Battelle Memorial Institute, Richland, Washington

Prepared under Contract NAS3–00137

National Aeronautics and
Space Administration

Glenn Research Center

June 2001

Available from

NASA Center for Aerospace Information
7121 Standard Drive
Hanover, MD 21076

National Technical Information Service
5285 Port Royal Road
Springfield, VA 22100

Available electronically at http://gltrs.grc.nasa.gov/GLTRS

# Normal Gravity Testing of a Microchannel Phase Separator for Insitu Resource Utilization

Ward E. TeGrotenhuis and Victoria S. Stenkamp
Battelle Memorial Institute, Pacific Northwest Division
P.O. Box 999, 3200 Q Avenue
Richland, Washington 99352

## Summary

Micro chemical and thermal systems (microCATS) is a general approach for reducing the size and mass of process hardware for a given processing rate. This value proposition is important for space applications, and efforts are underway to explore how the technology can be exploited in the continuing pursuit of human exploration and development of space. In particular, Battelle is working to develop the technology to support endeavors for in situ resource utilization.

Results are reported for experimental testing of a microchannel phase separator device that is expected to operate effectively in reduced gravity environments. Hydrodynamic, interfacial, and capillary forces will dominate over gravitational effects in microchannels that are less than 100 microns up to a couple of millimeters. The particular device tested here employs a microchannel having 2.7 millimeters as the smallest dimension, and a pore throat structure for capturing and removing liquid from a gas-liquid stream.

The microchannel device was tested in a horizontal orientation to minimize the influence of gravity at a wide range of gas and liquid flow rates ranging from 0.0005 up to 0.14 volume fraction of liquid. Four liquids were tested with air, in order to vary potentially important parameters, such as the Bond number and the Suratman number.

Results confirm that the biggest factor affecting the throughput capacity of the device is the capacity of liquid flow through the pore throat, which is dictated by permeability, liquid viscosity, flow area, pore throat thickness, and pressure difference across the pore throat. Typically, complete separation of gas and liquid fractions was lost when the liquid flow rate reached about 40-60% of the pore throat capacity. However, this could occur with as little as 10% utilization of pore throat capacity, and as great as 90% utilization.

The extent of pore throat utilization was also influenced by the expected two-phase flow pattern in the gas channel, as supported by correlations found between the utilization of pore throat capacity and two dimensionless parameters, the Suratman and the ratio of gas to liquid Reynolds numbers. Comparing the flow region where breakthrough of liquid occurs in the microchannel phase separator to the annular to plug flow transition of two-phase microgravity pipe flow reveals a high degree of correlation. This implies that a key to device performance is operating in the proper flow regime.

Analysis of the results indicate that the Bond number was not a significant factor in affecting performance, supporting the premise that hydrodynamic, interfacial, and capillary forces are more important than gravity. Therefore, the technology is applicable to space applications. However, the relative importance of gravity is better discerned through testing under reduced gravity conditions.

## Introduction

The NASA In Situ Resource Utilization (ISRU) program has overall objectives for developing opportunities for 'living off the land' in future space and planetary exploration missions [1,2]. Successful use of space resources represents large potential cost savings. Examples of consumables that may be produced from in situ resource includes propellants, fuels for rovers and power systems, materials for environmental control and life support system, materials supporting science activities, construction

materials, and commercial products. One near-term opportunity is the production of propellants from the carbon dioxide and possibly water in the Martian environment. The launch mass of sample return and human exploration missions can be dramatically reduced by not having to bring from earth all of the resources necessary for the outbound and the return flights [3]. Meeting ISRU objectives requires development of chemical and mechanical processing technologies that are suitable for space environments. Obviously, extraterrestrial processing plants will need to be compact, lightweight, efficient, and able to operate reliably for prolonged periods in reduced gravity environments.

For several years, Battelle has been developing micro chemical and thermal technologies (microCATS) using proprietary sheet architecture [4,5]. Microchannel heat exchangers, reactors, solvent extractors, and gas absorbers have been built and tested with evidence for dramatic improvements in performance over conventional technologies. The fundamental concept behind the approach is to engineer and fabricate devices with reproducible features and dimensions at the microscale, which reduces the length-scale for heat and mass transfer to 100 microns or less. The resulting dramatic increase in the rate of heat and mass transfer translates into reduced residence times, which in turn shrinks equipment size. These concepts have been demonstrated at Battelle and elsewhere [6-8].

Although the technology was conceived as a means for miniaturizing process technology by achieving superior heat and mass transfer over conventional hardware, the technology is also enabling when gravity is not available as a significant force. Reduced size and weight are obviously advantages for space exploration, but the small dimensions and high surface area to volume ratios in these devices implies the role of gravity diminishes in favor of capillary, surface, and hydrodynamic forces. This enables chemical processing in microgravity environments. In order to realize the potential of the technology for space applications, a fundamental understanding of the relative importance of forces is necessary in order to engineer process technology for microgravity and reduced gravity environments. The challenge remains in engineering devices at sufficiently small dimensions to take advantage of interfacial, surface, and hydrodynamic forces to achieve the same purposes with compact, lightweight, efficient hardware.

This report represents efforts in applying microCATS concepts for fluid phase separation—separating mixtures of immiscible fluids. There are numerous opportunities for phase separation technologies in space applications, such as water management in ECLSS (environmental control and life support systems) and in thermal systems involving phase change (Rankine cycle, vapor compression cycle, and heat pipes), and storage and transfer of cryogenic fluids [9]. The Mars In Situ Propellant Production (ISPP) plant requires water recovery and recycle, which can be accomplished by condensation followed by phase separation [2].

The microchannel architecture for phase separation is relevant for other technologies involving multi-phase flows. One example is recovery of condensable components from a vapor-gas mixture by partial condensation. This is accomplished by incorporating heat exchange channels for cooling the stream below the dew point. The architecture facilitates phase separation within a condensing heat exchanger that will work in reduced gravity environments. Other potential applications include gas absorption, stripping, and distillation.

Phase separation technologies necessarily involve processing a multi-phase fluid stream, which can involve very complex flow behaviors. Two-phase flow can take many different forms, including bubbly flow, slug flow, churn flow, annular flow, and stratified flow, depending on the particular flow regime as established by the relative flow rates, fluid properties, and forces at play [10]. A great deal of work has been performed on establishing flow maps to predict flow transitions for two-phase flow in various geometries, and seven to nine dimensionless groups have been identified as potentially important [11-13]. In addition, the relevance of two-phase flow phenomena in space technology and the unknowns associated with the change in behavior in the absence of gravity has generated extensive research into the influence of gravity, including a wide range of microgravity experiments [14,15].

The objective of developing microchannel phase separation technology suitable for space applications is to utilize only capillary, hydrodynamic, and surface forces to remove or recover a dispersed fluid phase from a second immiscible phase—the same principles apply to droplets dispersed in a liquid (emulsion), gas dispersed in a liquid (bubbles), or liquid dispersed in a gas (aerosol). Several technologies have been

developed previously for accomplishing phase separations in space. These broadly fall into two categories, static and rotary [9]. Rotary technologies rely on generating artificial body forces either by rotating equipment or by generating vortex flows. Static devices rely on other forces, such as wetting and capillary force, to separate mixed fluid phases. Many of these devices employ wicks and porous materials to achieve separation and to direct the fluids to the appropriate outlets. The microchannel separator being investigated also employs some of the same principles. However, the intent is to enhance the hydrodynamic, capillary, and surface forces by performing the phase separation in channels having a very small hydraulic diameter. Success is measured by achieving very high throughput per unit hardware volume, thereby reducing the size and weight of the hardware required for a given application.

## Technology Description and Theory of Operation

The fundamental approach for the microchannel phase separation technology is to utilize capillary, surface, and hydrodynamic forces to collect one of the phases into specific flow regions while excluding the other. The technology is described for gas-liquid separation, but is also applicable to liquid-liquid separation by analogy. In the general conception of the technology, phase separation is accomplished using combinations of capture, wicking, and pore throat structures within the microchannels as depicted in Figure 1. The gas-liquid mixture enters the device and flows through the region containing the capture structure. Capillary, surface, and hydrodynamic forces cause the liquid phase to come into contact and preferentially sorb into the adjacent wicking / pore throat structure. The pore throat / wick structure provides a path for the liquid to flow to a liquid outlet while precluding gas intrusion. The gas phase exits from a separate outlet. The architecture can be tailored for a particular application depending on the volume fractions of the phases, the degree of dispersion in the feed including the particle size distribution if one phase is disperse, and external system constraints such as pressures. Figure 1 shows a co-current flow arrangement, but either co-current or counter-current is possible. The microchannel phase separation technology is scaled-up to higher volumetric flows by stacking alternating layers of gas (capture structure) and liquid (wick / pore throat) microchannels.

The microchannel architecture constrains the smallest channel dimension (width) to be less than 1 mm down to less than 100 microns, which causes surface forces and hydrodynamic forces to dominate gravitational forces. The region containing the capture structure is designed to induce contact between the liquid phase and the wicking / pore throat structure. For cases where both phases are relatively continuous (annular or slug flow regimes), the capture structure can be an open microchannel and hydrodynamic forces induce the contact.

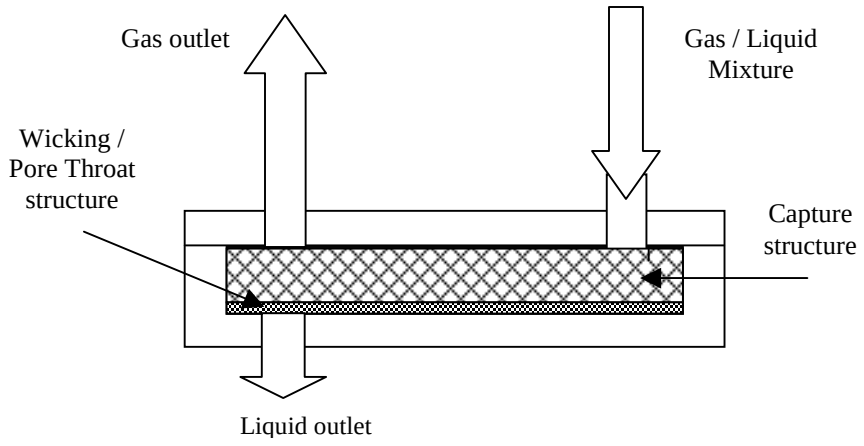


**Figure 1. Schematic of a single-channel-pair microchannel phase separator employing a wicking structure for capturing the liquid phase and an optional capture structure in the gas channels.**

The wicking / pore throat structure provides a flow path for the separated liquid phase. Two mechanisms are required for the device to operate effectively, a wicking mechanism and a mechanism for excluding gas. The wicking mechanism is accomplished by a porous structure that is wetting for the liquid in order to cause preferential sorption, while having high permeability to provide flow capacity to the outlet. The second mechanism is also required to prevent intrusion by the gas stream into the liquid outlet channel, and is accomplished using a pore throat. The bubble point of the pore throat, as dictated by the maximum pore size, contact angle, and surface tension of the liquid, determines the maximum allowable pressure differential between the gas and liquid outlets. The wick and the pore throat can be embodied in the same component or structure.

The purpose of the testing reported here is to determine the performance characteristics of the architecture, to identify key principles and parameters, and to develop scaling relationships. The processing capacity of the device is constrained by a number of parameters, some of which are explored by the test results presented below. The failure modes are breakthrough of the liquid phase into the gas outlet and intrusion of gas into the liquid outlet. The longer-term objectives are to determine the residual effects of Earth's gravity and the importance of unmasked phenomena.

One of the factors limiting the processing capacity of the device is how effectively the liquid phase is brought into contact with the wicking structure. For an open rectangular microchannel, this removal effectiveness is expected to depend on the flow regime encountered in the device. Annular and stratified flow will bring the liquid into contact with the walls, allowing it to siphon through the liquid flow channel to the liquid outlet. The likelihood of having breakthrough of liquid to the gas outlet increases as the flow transitions toward a regime where the liquid is entrained in the gas flow, such as in slug flow or wispy annular flow. Therefore, the ability to recover water from the gas stream is expected to correlate with parameters that are typically used to characterize flow regime transitions. Three such parameters are the ratio of the gas and liquid Reynolds numbers, $Re_{GS}/Re_{LS}$ where $Re_{GS} = \rho_G U_{GS} D_h/\mu_G$ and $Re_{LS} = \rho_L U_{LS} D_h/\mu_L$ [13]. Other useful dimensionless groups are the ratio of the viscosities, $\mu_L/\mu_G$, the Capillary number, $Ca = \mu_L U_{LS}/\sigma$, characterizing the relative importance of viscous to surface tension forces, the Weber number, $We = \rho_L U_{LS}^2 D_h/\sigma$, the Suratman number, $Su = \sigma D_h \rho_L/\mu_L$, and the Bond number, $Bo = (\rho_L - \rho_G) g D_h^2/\sigma$, indicating the relative importance of gravity forces to surface tension forces.

Another factor limiting the throughput of the device is the flow capacity of the wicking and pore throat structure. This porous structure is characterized by a permeability coefficient defined as,

$$K = \frac{\mu_L \, h \, Q}{A \, \Delta P} \tag{1}$$

where $Q$ is the volumetric flow of fluid through the cross-sectional area $A$, of a porous media of thickness $h$, under an applied pressure drop of $\Delta P$. The pore throat maximum liquid flow capacity, $Q_{pt}$, is then calculated for a given experiment from the viscosity of the liquid and the pressure difference across the pore throat structure. Device performance can then be characterized by the volumetric flow of recovered liquid as a percentage of the pore throat maximum flow capacity.

A third potential limiting factor is intrusion of gas into the pore throat, which can occur at the bubble point of the pore throat, which is calculated from the Young-Laplace equation,

$$\Delta P_{\max} = \frac{2\sigma \cos(\theta)}{r_p} \tag{2}$$

where $\theta$ is the contact angle between the liquid and the pore throat and $r_p$ is the maximum pore radius.

**Experimental Apparatus and Procedure**

The device tested employed a single microchannel. The gas flow channel was 7.3 cm x 1.4 cm x 0.27 cm, while the adjacent liquid channel was 8 cm x 2 cm x 0.036 cm. The gas channel was open and did not contain a capture structure. Polymethyl methacrylate (Plexiglass™ or Lucite™) bounded one interior face of this channel while the pore throat of the liquid channel bounded the opposing face. The liquid channel consisted of Pall Supramesh Z (0.003 mm thick) overlying a 70-mesh stainless steel screen (0.033 mm thick). Pall Supramesh Z is comprised of sintered stainless steel bonded to a fine stainless steel mesh. The remaining interior faces of the device were polycarbonate. This configuration gives the maximum pore throat area, which allows the maximum capacity of liquid flow and does not employ a separate wicking structure per se. The device was tested while oriented horizontally to minimize the effects of gravity with the gas channel located above the liquid channel.

To allow pressure and temperature measurements of the streams, thermocouples (Type K) and oil filled pressure transducers (Paroscientific model 2100A-102) were placed at the inlets and outlets of the device. The pressure transducers have an accuracy of ±0.01 psi. Both the pressure and temperature were measured at the entrance and gas outlet of the device. At the liquid outlet, only the temperature was measured, while the pressure was calculated. The pressure transducers were placed as close to the device as possible.

A mass flow controller and a peristaltic pump were used to supply the gas and liquids, respectively, through 1/8-inch tubing to a T-fitting where the phases were mixed. The two-phase stream proceeded through additional 1/8-inch tubing, through thermocouple and pressure transducer fittings, and into the device through a 4.7 mm opening. The gas and liquid flow rates coming from the gas outlet were measured using the quantification system depicted in Figure 2. As the flow exits the device, it enters a flask for recovering any entrained liquids droplets. The gas continues through the total volumetric flow. The quantity of liquid exiting during a run is determined gravimetrically since both the flask and drying agent are placed on a scale. The flowrate of air is determined as the difference between the total and liquid flowrates. Calibrations were performed whereby the device was removed and known flowrates introduced to the quantification system. The results indicate that the measured flowrate of air is accurate to within 5%. Gas breakthrough from the liquid exit was a drying agent then a flowmeter for measuring monitored by feeding the liquid outlet stream into an inverted graduated cylinder filled with test liquid, and the total amount of entrained gas over a given period of time was measured by displacement. The time-average gas flow of entrained gas coming out of the liquid outlet was calculated. The flow rate of liquid coming out of the liquid outlet was typically calculated by difference, but was also measured independently in some cases.

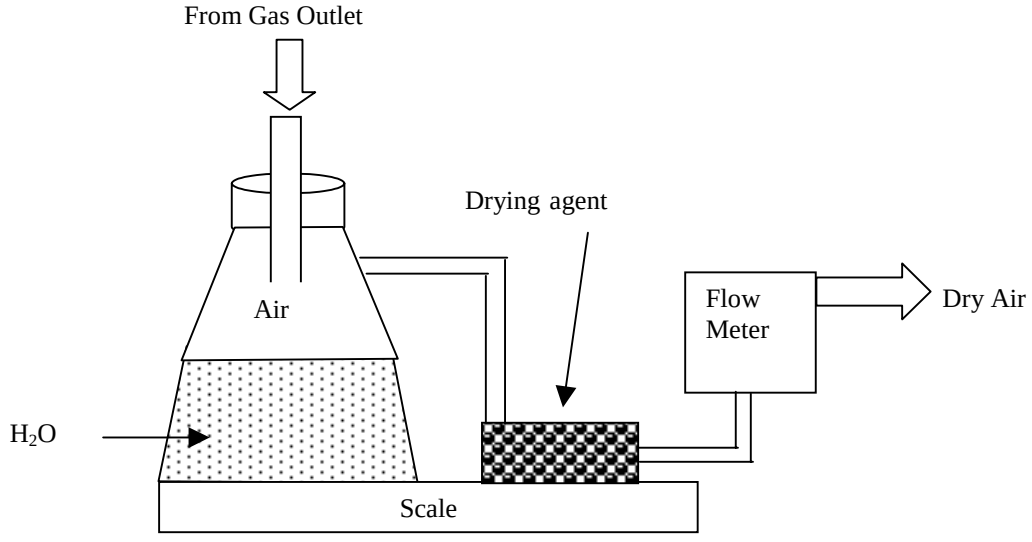


**Figure 2. Schematic of system to quantify air and liquid flow rates coming from the gas outlet.**

The pressure difference across the pore throat is one of the critical operating parameters. Its value was adjusted by controlling the siphon pressure at the liquid outlet. This was done by submerging the liquid discharge line into a bath of constant height and raising and lower the bath. Corrections were made for the backpressure created by the gas stream quantification system and the friction losses in the liquid discharge line. The pressure difference across the pore throat could be controlled very well when there was no breakthrough of liquid to the gas outlet. Once breakthrough occurred, the resulting two-phase flow in the gas outlet line and quantification system would cause an increase in back pressure that could not be anticipated as well as pressure fluctuations of several inches of water. At this point, control of pressure difference across the pore throat became problematic and the height of the liquid discharge bath was no longer adjusted.

All experiments were performed with air as the gas phase. Four different liquids were used in order to vary the fluid properties, thereby altering dimensionless groups, including Bo, We, Ca, Su, and the viscosity ratio. In addition to water, 4 cP and 14 cP glycerin/water mixtures, and decane were used for the liquid phase. Properties and dimensionless groups are given for each of the liquids used in testing in Table A.2 of Appendix A.

## Results and Discussion

The experiments were designed to explore the performance of a single-channel microchannel phase separator as a function of gas and liquid flow rates, the pressure difference across the pore throat, and liquid physical properties. A single configuration was tested that was designed to operate at relatively low liquid phase volume fraction, and was tested over the range from 0.05% up to 14%.

*Liquid Breakthrough* - Experimental series were run by varying the liquid flow rate, while keeping the gas flow rate and pressure difference across the pore throat relatively constant. However, as soon as the liquid broke through to the gas outlet, the subsequent two-phase flow in the apparatus down stream of the gas outlet would cause large fluctuations in the backpressure to the device, making it problematic to control the pressure difference across the pore throat. Figure 3 gives results for recovery of water at a target pressure difference of 12 inches of water column. Each set of symbols represents a constant gas volumetric flow (standard conditions). Liquid flow is increasing from right to left, and when the water recovery drops below 100%, the pressure difference across the pore throat increases due to the increasing backpressure on the gas outlet. As expected, at some critical liquid flow rate, breakthrough of water occurred at the air exit. The liquid flow rate at breakthrough decreases with increasing gas Reynolds number.

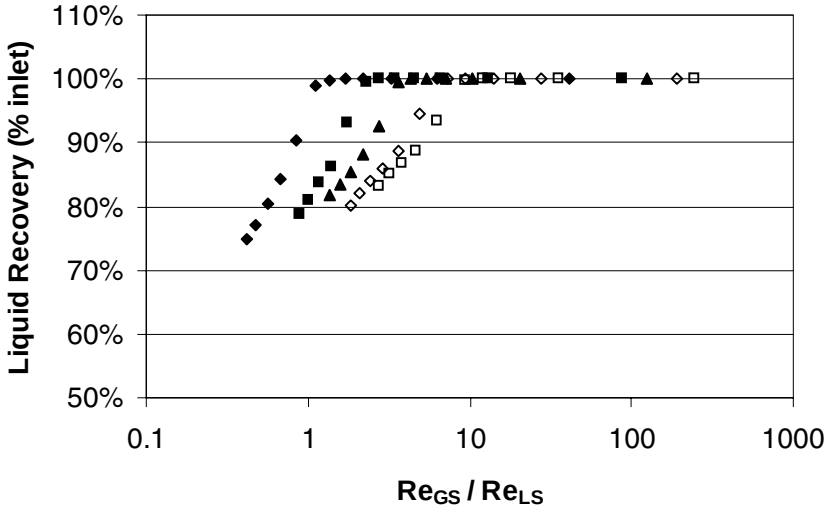


**Figure 3. Percent of feed water recovered from the liquid outlet as a function of $Re_{GS}/Re_{LS}$ with a target pressure difference of 12 inches water across the pore throat for gas Reynolds numbers of $Re_{GS}$ ~ 125 (◆), $Re_{GS}$ ~ 250 (■), $Re_{GS}$ ~ 390 (▲), $Re_{GS}$ ~ 525 (◇), $Re_{GS}$ ~ 675 (△).**

When 100% separation of the liquid from the gas stream occurred, the pressure drop from the inlet to the gas outlet was a fraction of an inch of water column even at the highest processing rates tested. The measured pressure drop was less than the accuracy that could be achieved with the pressure transducers. Once breakthrough of liquid into the gas outlet occurred, the subsequent two-phase flow down stream of the device caused backpressure fluctuations as high as 6-12 inches water column, which were much greater than the pressure drop across the device.

Observations were made of the flow behavior in the device. For a given gas flow rate and pressure difference across the pore throat, there was no discernible hold-up of liquid in the gas channel at low liquid flow rates. The small fraction of liquid would quickly sorb into the pore throat and be siphoned from the device. This condition is depicted in Figure 4, for flow rates of 2 mL/min of water and 1 SLPM of air with a pressure difference across the pore throat of 12 inches of water. As the liquid flow rate was increased, liquid would begin to accumulate around the edges of the channels, at the entrance and along the sides as seen in Figure 5 for flow rates of 40 mL/min of water and 1 SLPM of air with 12 inches of water pressure drop across the pore throat. This accumulation would grow as the liquid flow was increased further, reducing the flow area for gas. Eventually, the shear forces at the gas liquid interface would be sufficient to cause entrainment of liquid into the gas leaving the device. For example, entrainment occurred at conditions of 130 mL/min of water flow, 1 SLPM air flow, and 12 inches of water pressure drop targeted across the pore throat, which is shown in Figure 6.

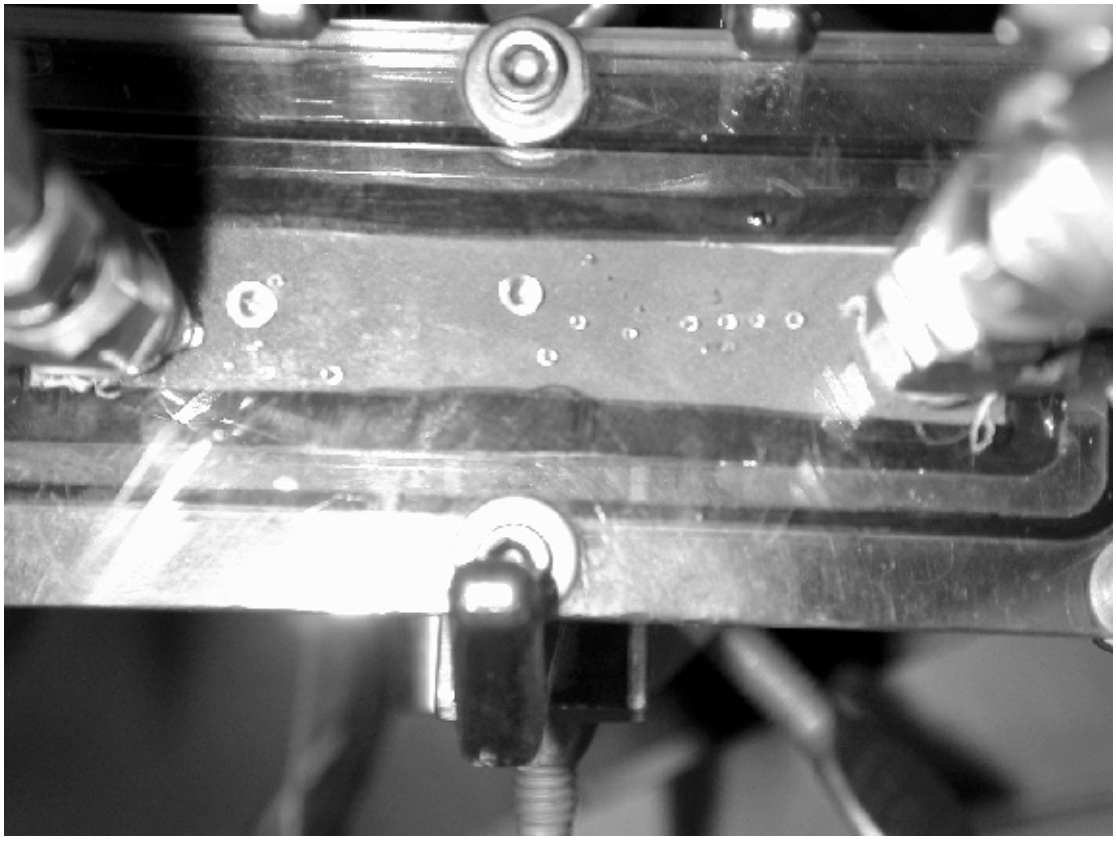

**Figure 4. View of device top with flow rates of 2 mL/min of water and 1 SLPM of air. The pressure drop across the pore throat is 12 inches of water. No breakthrough is observed**.

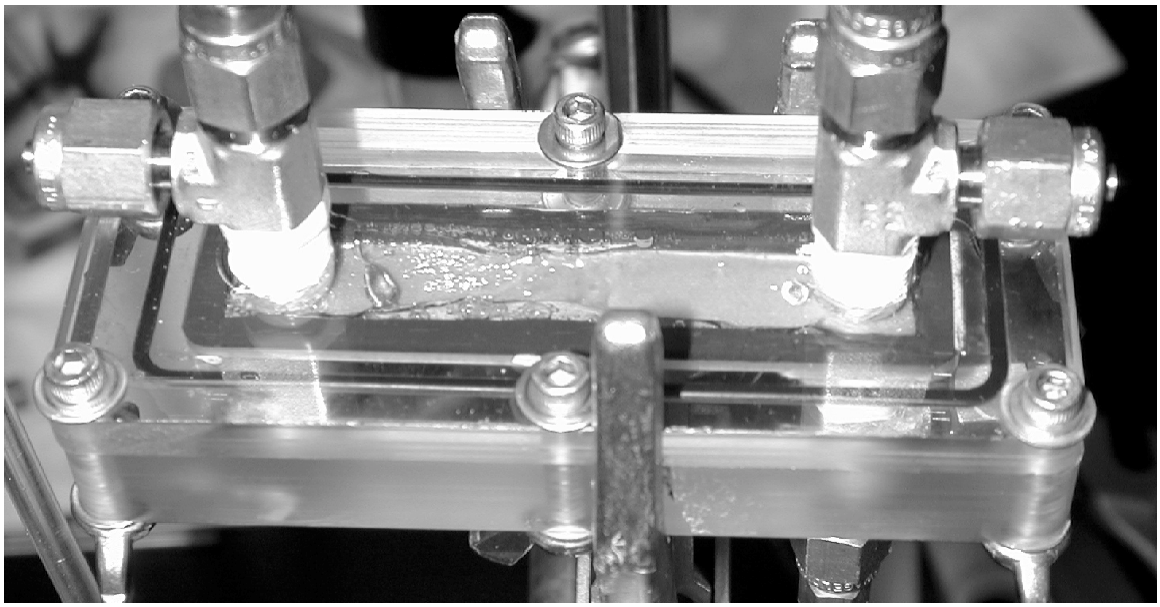

**Figure 5. Device running at flow rates of 40 mL/min of water and 1 SLPM of air. The pressure drop across the pore throat is 12 inches of water. No breakthrough is observed.**

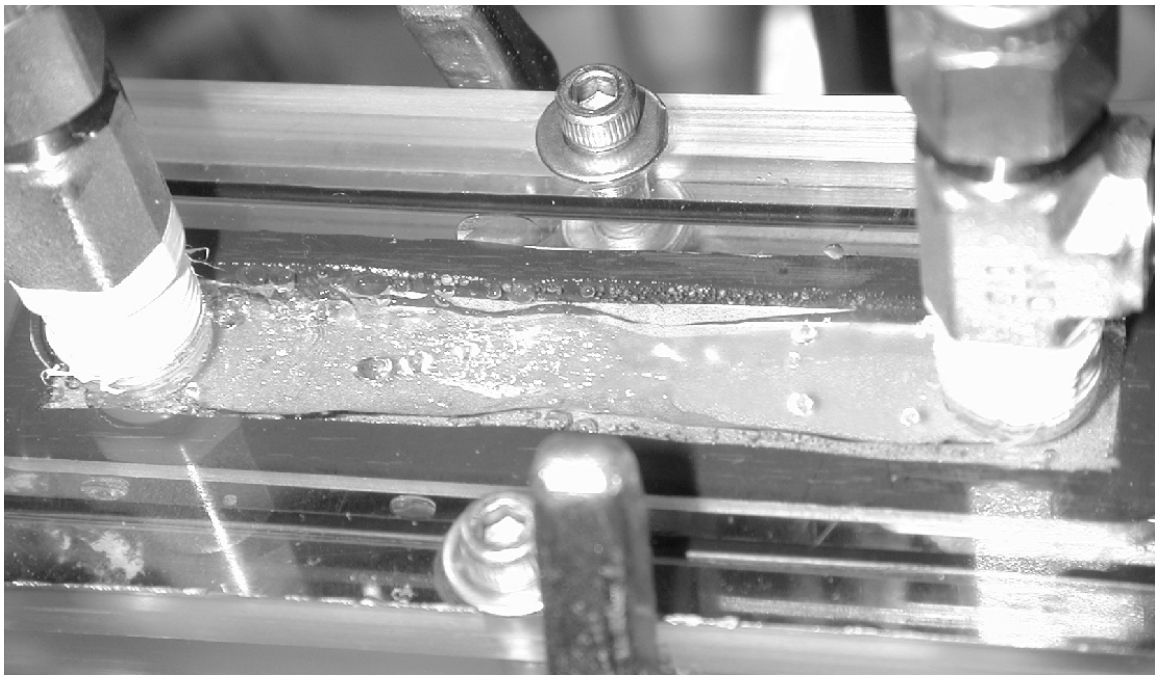

**Figure 6. Device running at flow rates of 130 mL/min water and 1 SLPM air. The pressure drop across the pore throat is 12 inches of water. Breakthrough is observed.**

The effect of viscosity was evaluated by testing the device with water (1 cP) and two glycerin-water mixtures (4 cP and 14 cP). Changing the viscosity was found to have a profound influence on the liquid recovery, as shown in Figure 7 for the three liquids at constant gas Reynolds number. Increasing the viscosity decreases the maximum liquid flow rate that can be accommodated before breakthrough, thus shifting the point where the liquid capacity falls below 100% to the right on the graph.

Changing the surface tension of the liquid had a much less profound effect than viscosity as shown in Figure 8. Both decane ($\sigma$ = 23 dynes/cm) and water ($\sigma$ = 72 dynes/cm) were evaluated. In each case, the difference in performance is fairly similar, with breakthrough occurring at slightly higher liquid flow rates for decane, thus shifting these curves to the left of the water curves. Figure 8 also illustrates that increasing the pressure drop across the pore throat increases the liquid capacity of the device, thus moving the curve to the left. This can be seen by comparing the curves for $Re_{GS}$ = 380 for both 6" (diamonds) and 18" (triangles) pressure drops across the pore throat.

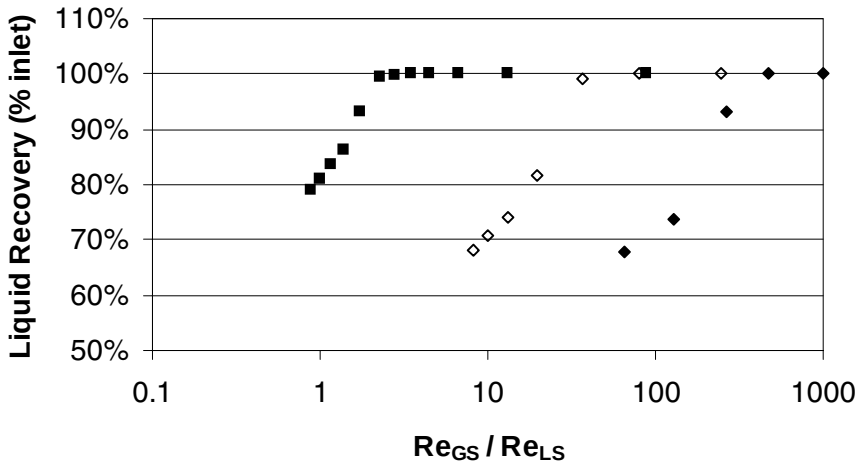


**Figure 7. Percent of feed water recovered from the liquid outlet as a function of $Re_{GS}/Re_{LS}$ with a target pressure difference of 12 inches water across the pore throat for liquid viscosities of 1 cP(■), 4 cP (◇), and 14 cP(◆).**

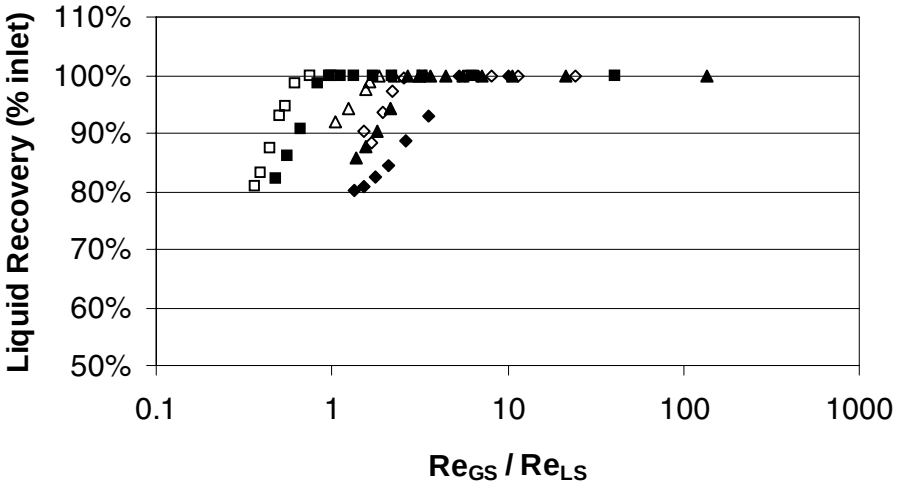


**Figure 8. Percent of feed water recovered from the liquid outlet as a function of $Re_{GS}/Re_{LS}$ with varying surface tensions and various targeted pressure differences across the pore throat:**

**72 dynes/cm, 18 in. WC, $Re_{GS}$ = 125 (■)**
**23 dynes/cm, 18 in. WC, $Re_{GS}$ = 125 (□)**
**72 dynes/cm, 18 in. WC, $Re_{GS}$ = 390 (▲)**
**23 dynes/cm, 18 in. WC, $Re_{GS}$ = 390 (△)**
**72 dynes/cm, 6 in. WC, $Re_{GS}$ = 390 (◆)**
**23 dynes/cm, 6 in. WC, $Re_{GS}$ = 390 (◇)**

*Gas Breakthrough* - In all cases, gas breakthrough to the liquid outlet was minimal. Average gas flow from the liquid outlet did not exceed 1.4% of the feed gas flow as depicted in Figure 9. Theoretically, gas breakthrough should not occur until the bubble point pressure is exceeded. Bubble point is defined as the maximum pressure difference that can be sustained across the media without gas intruding through the media and displacing the media. The bubble point is calculated from the Young-Laplace equation (Equation 2), and is determined by the maximum pore size, surface tension, and the receding contact angle. The maximum pore size for Pall Supramesh Z material is estimated to be 15 micron in diameter, based on the reported 100% removal rating. Measured surface tensions and receding contact angles as well as the calculated bubble point pressure are given in Table 1 for the fluids tested. The intended pressure difference across the pore throat was kept below the bubble point in order to avoid gas intrusion. The gas intrusion rate as a percentage of the feed gas flow rate is plotted in Figure 9 as a function of the pressure difference across the pore throat (as a percentage of the bubble point pressure). As can be seen, gas breakthrough can occur with water and glycerin-water solutions at approximately 50-60% of the bubble point pressure. In the majority of cases, breakthrough of gas in the liquid outlet occurs only when liquid breaks through to the gas outlet. The 6 to 12 inches of water pressure fluctuations that occur with liquid breakthrough can explain why gas breakthrough is seen at pressure differences significantly below the bubble point pressure. In the case of decane, breakthrough starts to occur at values close to the bubble point pressure. Decane is assumed to have a zero receding contact angle, which may over predict the bubble point. In addition, inaccuracies in the calculated bubble point pressure due to inaccuracies or variations in the contact angle or maximum pore size could account for the early breakthrough and the differences in behavior with decane versus the other liquids.

**Table 1. Surface tension, receding contact angle, and theoretical bubble point of various fluids interacting with Pall Supramesh Z material.**

| Fluid | Surface Tension σ (Dynes/cm) | Receding Contact Angle θ (degrees) | Theoretical bubble point (in. WC) |
|---|---|---|---|
| Water | 72 | 41 | 58 |
| 4 cP Glycerin / Water | 70 | 41 | 56 |
| 14 cP Glycerin / Water | 67 | 45 | 50 |
| Decane | 23 | 0 | 25 |

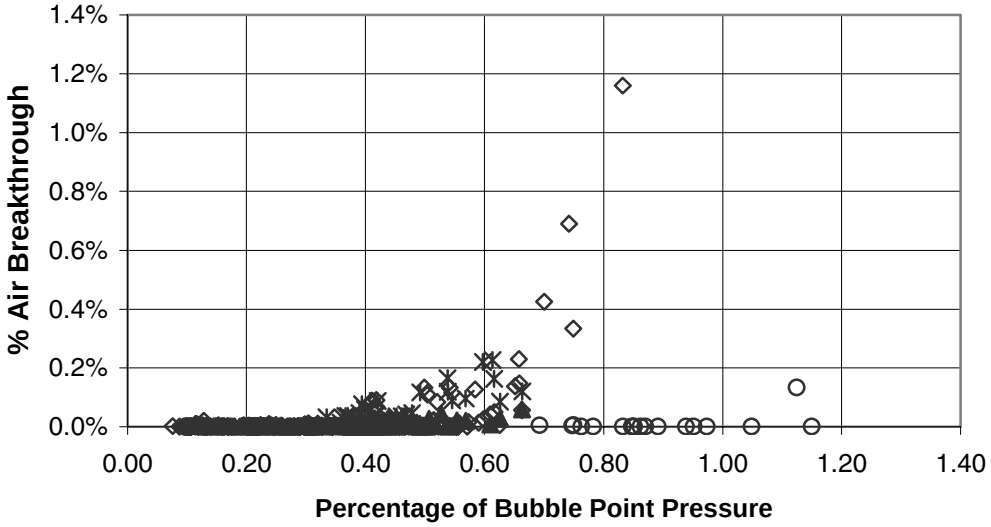


**Figure 9. Average breakthrough of gas to the liquid outlet as a percentage of the feed gas flow plotted as a function of the pressure difference across the pore throat expressed as a percentage of the bubble point pressure (◇Water; ✳ 4 cP Glycerin; ▲14 cP Glycerin; ○Decane).**

*Correlation with Dimensionless Parameters* – Knowing which dimensionless groups (such as Ca, We, Su, Bo) affect the performance of the device, as well as knowing which groups have no discernible effect, provides insight into what forces and physical mechanisms are at work in making the device function as intended. To determine which dimensionless groups are important, the aforementioned groups can be correlated as a function of the device performance. One measure of the device performance is the maximum liquid flow rate that could be processed without breakthrough at a given gas flow and pressure difference across the pore throat. Instead of locating this point experimentally, this maximum liquid flow rate was calculated using linear regression of the water flow from the gas outlet versus the liquid feed flow in the region where breakthrough for the liquid is occurring. The intercept of the regression yields the calculated maximum liquid flow rate, $Q_{max}$. In actuality, a small amount of liquid breakthrough was observed at liquid flowrates lower than the calculated maximum. This is represented by a 'knee' in the liquid recovery versus $Re_{GS}/Re_{LS}$ curves, such as those shown in Figure 3. It is observed that the region around the incipient breakthrough point is unstable, and it is presumed that small perturbations, such as those in pressure or flow, can yield an occasional loss of liquid out the gas outlet. Consequently, a design of a device for a given application would require a margin of over design to avoid this region of instability.

The maximum liquid flow rate is necessarily constrained by the capacity of the pore throat material, as represented by $Q_{pt}$ calculated from Equation 1. The permeability of the pore throat was determined from flow experiments where the gas channel of the separator device was filled with water at a constant head pressure and the liquid flow out of the liquid outlet was measured. Permeability was then calculated using Equation 1 at several pressures and the results are shown in Figure 10. From these results, a value of $1.8 \times 10^{-10}$ cm$^2$ was used as the permeability, $K$, in subsequent calculations of $Q_{pt}$.

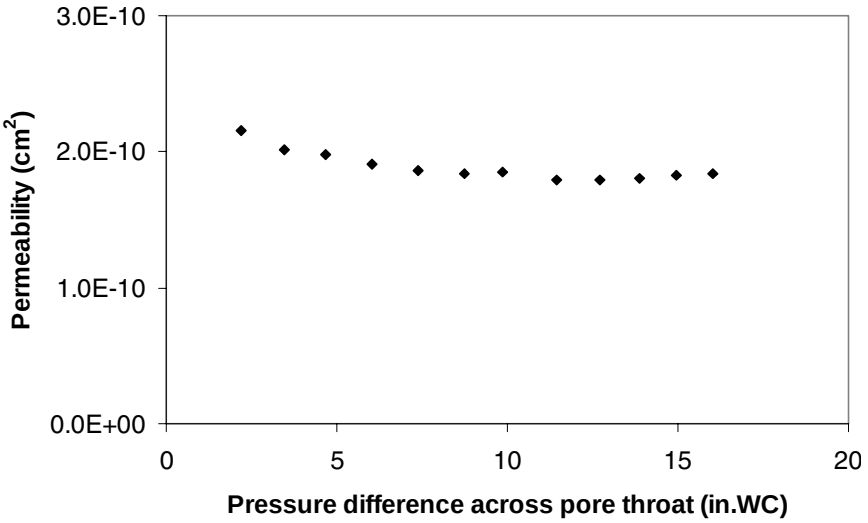


**Figure 10. Permeability of the pore throat measured as a function of the pressure difference across the pore throat.**

A dimensionless measure of performance is the liquid recovery as a percentage of the pore throat capacity, calculated as $Q_{max}/Q_{pt}$. The maximum liquid flow rate, the pore throat capacity, and the percent ratio are summarized in Table A.1 in Appendix A for the various conditions and liquids tested, along with values for several dimensionless groups. Using the value of $Q_{max}/Q_{pt}$ provides a good comparison of all data, since it normalizes the strong effect of viscosity and pressure difference across the pore throat. For example, the values of $Q_{max}/Q_{pt}$ for water (1 cP) and the water/glycerin mixtures (4 cP and 14 cP) at conditions shown in Figure 7 are 0.50, 0.74, and 0.72, respectively, which are comparable.

A series of analyses were performed looking for statistically significant relationships between dimensionless parameters and the device performance ($Q_{max}/Q_{pt}$). Several combinations of parameters were found to be statistically significant, but the combination that gave the highest probabilities for significance was $\ln(Re_{GS}/Re_{LS})$ together with $\ln(Su)$. Statistical least squares analysis gave greater than

99.99% probability that these two quantities in combination affect the performance of the device in influencing water breakthrough. The Bond number did not have a significant effect on performance in the particular configuration and orientation that was tested. This lack of correlation supports the original premise that interfacial, capillary, and hydrodynamic forces rather than gravitational forces would dominate two-phase flow in a microchannel. This lack of correlation occurs since the surface tension was observed to have only a minor affect on the liquid capacity (Figure 8), therefore this conclusion would be better supported through testing under microgravity conditions.

The dependence on the Suratman number may be understood in the context of two-phase flow regimes. For the device to operate with complete separation, not only must fluid be transported through the pore throat, but in addition, mechanisms must exist to remove the liquid from the flowing gas and prevent the shear forces at the gas-liquid interface from entraining the liquid. Annular, stratified, and perhaps wavy flow would be expected to facilitate effective separation. Slug, bubbly, churn, or wispy annular flow patterns would allow entrainment and breakthrough of liquid to the gas outlet.

The ratio of the Reynolds numbers $Re_{GS}/Re_{LS}$ and the Suratman number are known to be important parameters in characterizing transitions in flow pattern mapping [13]. For example, the value of $Re_{GS}/Re_{LS}$ where the transition from annular to slug flow occurs in microgravity two-phase pipe flow is proportional to $Su^{-2/3}$ when $Su<10^6$ [13]. This transition occurs between $Re_{GS}/Re_{LS}=1$ and 10 as shown by the line in Figure 11. A summary of data for incipient breakthrough data for the microchannel gas-liquid separator is also shown in Figure 11. A similar dependence on the Suratman number is found, which shows a decrease with the Reynolds number ratio. This similar correspondence thus suggests that a transition from annular to slug flow is a contributing factor for causing incomplete separation. In future experiments, video may aid in firmly establishing the importance of the flow regime.

As mentioned above, the permeability of the pore throat material is a critical parameter in establishing the maximum liquid processing capacity of the device. The same piece of pore throat material was used for all of the experiments. In addition, care was taken to periodically clean the pore throat material to prevent potential build-up of material in the pores causing reduced permeability. Despite the steps taken to maintain constant permeability, variation in permeability is a likely source of the scatter in the data and problems with irreproducibility.

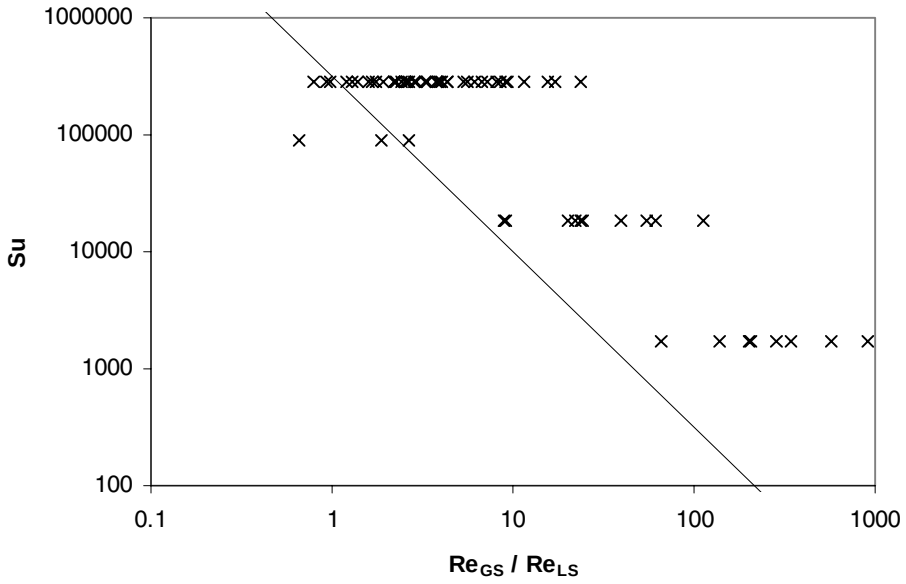


**Figure 11. Map of the transition to breakthrough of liquid out of the device as determined by the Suratman number and the ratio of the gas to liquid Reynolds numbers. The line corresponds to the slug-annular transition found for two-phase pipe flow in microgravity [13].**

## Conclusions

The performance of a single-channel microchannel phase separator device was successfully tested. The device employs a pore throat structure within a microchannel. Four fluids were used having varying viscosities and surface tensions in order to discern the relative importance of hydrodynamic, interfacial, and gravitational forces as characterized by dimensionless groups such as the Reynolds numbers, the Bond number, and the Suratman number.

The most important factors governing performance relate to the flow capacity of the pore throat structure, including the pore throat permeability, pressure difference across the pore throat, and the viscosity of the liquid. Therefore, the most effective way of increasing processing capacity for a given process stream would be to increase flow capacity of the pore throat.

Breakthrough of gas to the liquid outlet was not problematic, but a small fraction of gas entrainment in the liquid was observed at pressure differences below the bubble point pressure for the pore throat. The most likely cause was fluctuations in the backpressure on the gas outlet, which became several inches of water when liquid breakthrough to the gas outlet occurred.

Results also indicate that performance is effected by the pattern of two-phase flow in the gas channel. Breakthrough of liquid to the gas outlet occurs in the same flow region where a transition occurs between annular and slug flow for two-phase flow in a pipe in microgravity. Breakthrough can occur when flow through the pore throat reaches 10-90% of the flow capacity, depending on the ratio of the gas and liquid Reynolds numbers and the Suratman number.

## Nomenclature

### *Dimensionless Groups*

$Bo = (\rho_L - \rho_G)\, g\, D_h^2 / \sigma$ -- Bond number
$Ca = \mu_L\, U_{LS} / \sigma$ -- Capillary number
$Re_{GS} = \rho_G\, U_{GS}\, D_h / \mu_G$ -- gas phase Reynolds number based on gas superficial velocity
$Re_{LS} = \rho_L\, U_{LS}\, D_h / \mu_L$ -- liquid phase Reynolds number based on liquid superficial velocity
$Su = \sigma\, D_h\, \rho_L / \mu_L$ -- Suratman number
$We = \rho_L\, U_{LS}^2\, D_h / \sigma$ -- Weber number

### *Symbols*

A -- cross sectional area
g -- acceleration due to gravity
$D_h$ -- hydraulic diameter (based on channel cross section)
h -- thickness of porous media
K -- porous media permeability
Q -- volumetric flow of fluid
$Q_{max}$ -- maximum liquid flow rate without breakthrough
$Q_{pt}$ -- maximum liquid flow capacity of the pore throat material
$r_p$ -- maximum pore radius
$U_{LS}$ -- liquid superficial velocity (based on air channel cross section and feed liquid flow)
$U_{GS}$ -- gas phase superficial velocity (based on air channel cross section and feed gas flow)

### *Greek Symbols*

$\Delta P$ -- applied pressure difference across the pore throat
$\Delta P_{max}$ -- maximum pressure difference that can be applied across the pore throat without gas intrusion
$\mu_G$ -- gas dynamic viscosity
$\mu_L$ -- liquid dynamic viscosity
$\theta$ -- contact angle of liquid against solid
$\rho$ -- density
$\rho_G$ -- gas density
$\rho_L$ -- liquid density
$\sigma$ -- liquid surface tension

**References**


1. Sanders, G.B., "ISRU: An Overview of NASA's Current and Development Activities and Long-Term Goals," AIAA 2000–1062, 38th Aerospace Sciences Meetings and Exhibit, Reno, NV, 2000.

2. TeGrotenhuis, W.E., R.S. Wegeng, D.P. Vanderwiel, G.A. Whyatt, V.V. Viswanathan, K.P. Schielke, J.B. Sanders, and T.A. Peters, "Microreactor System Design for NASA In Situ Propellant Production Plant on Mars," AIChE 2000 Spring National Meeting, Atlanta, GA, March 5–9, 2000.

3. Frankie, B.M. and R. Zubrin, "Chemical Engineering in Extraterrestrial Environments," Chem. Eng. Progress, **95**(2), 45–54, 1999.

4. Wegeng, R.S., M.K. Drost, C.J. Call, J.G. Birmingham, C.E. McDonald, D.E. Kurath, and M. Friedrich, "Microcomponent Chemical Process Sheet Architecture," U.S. Patent 5,811,062, 1998.

5. Wegeng, R.S., M.K. Drost, and C.E. McDonald, Microcomponent Sheet Architecture, U.S. Patent 5,611,214, 1997.

6. Drost, M.K., C.J. Call, J.M. Cuta, and R.S. Wegeng, "Microchannel Integrated Evaporator/ Combustor Thermal Processes." J. of Microscale Thermophysics Engineering, **1**(4), 321–333, 1997.

7. TeGrotenhuis, W.E., R. Cameron, M.G. Butcher, P.M. Martin, and R.S. Wegeng, "Micro Channel Devices for Efficient Contacting of Liquids in Solvent Extraction", Sep. Sci. Technol., **34**(6&7), 951–974, 1999.

8. Ehrfeld, W., V. Hessel, S. Kiesewalter, H. Lowe, Th. Richter, and J. Schiewe, "Implementation of Microreaction Technology in Process Engineering," Microreaction Technology: Industrial Prospects, Proceedings of the Third International Conference on Microreaction Technology, Springer, Berlin, 2000, pp. 14–35.

9. Dean, W.C., "Zero Gravity Phase Separator Technologies—Past, Present and Future," SAE Tech. Paper Ser. 911524, 21st Int. Conf. on Env. Systems, San Francisco, July 15–18, 1991.

10. Carey, V.P., *Liquid-Vapor Phase-Change Phenomena*, Hemisphere Pub. Corp., Washington, 1992.

11. Mandhane, J.M., G.A. Gregory, and K. Aziz, "Flow Pattern Map for Gas-Liquid Flow in Horizontal Pipes," Int. J. Multiphase Flow, **1**, 537–553, 1974.

12. Taitel, Y. and A.E. Dukler, "A Model for Predicting Flow Regime Transitions in Horizontal and Near Horizontal Gas-Liquid Flow," AIChE J., **22**, 47–55, 1976.

13. Jayawardena, S., V. Balakotaiah, and L.C. Witte, "Flow Pattern Transition Maps for Microgravity Two-Phase Flows," AIChE J., **43**(6), 1637–1640, 1997.

14. Bousman, W.S., "Studies of Two-Phase Gas-Liquid Flow in Microgravity," Ph.D. Diss., Univ. of Houston, 1994.

15. Dukler, A.E., J.A. Fabre, J.B. McQuillen, and R. Vernon, "Gas-liquid Flow at Microgravity Conditions: Flow Patterns and Transitions," Int. J. Multiphase Flow, **14**(4), 389, 1988.

**Appendix A**
**Summary of Results**

**Table A.1. Summary of results for the maximum liquid flow rate as a percent of the maximum capacity of the pore throat for the given pressure difference across the pore throat along with values for potential meaningful dimensionless groups.**

| Liquid [a] | $Re_{LS}$ | $Re_{GS}$ | $We_{LS}$ | Ca ($x10^5$) | $\Delta P$ [b] (in. WC) | $Re_{GS}/Re_{LS}$ | $Q_{max}/Q_{pt}$ [c] |
|---|---|---|---|---|---|---|---|
| Water | 95 | 130 | 0.032 | 34 | 7.8 | 1.4 | 72% |
| Water | 60 | 130 | 0.013 | 22 | 9.6 | 2.2 | 37% |
| Water | 100 | 270 | 0.036 | 36 | 7.4 | 2.6 | 80% |
| Water | 67 | 270 | 0.016 | 24 | 7.2 | 4.0 | 56% |
| Water | 51 | 410 | 0.009 | 18 | 6.9 | 8.1 | 43% |
| Water | 77 | 410 | 0.021 | 28 | 7.3 | 5.3 | 62% |
| Water | 76 | 550 | 0.021 | 27 | 6.0 | 7.2 | 75% |
| Water | 64 | 540 | 0.014 | 23 | 7.9 | 8.6 | 48% |
| Water | 45 | 700 | 0.007 | 16 | 5.6 | 16 | 47% |
| Water | 42 | 720 | 0.006 | 15 | 4.4 | 17 | 56% |
| Water | 110 | 130 | 0.042 | 39 | 11.6 | 1.2 | 55% |
| Water | 130 | 130 | 0.063 | 48 | 12.7 | 1.0 | 62% |
| Water | 110 | 270 | 0.044 | 40 | 12.3 | 2.4 | 53% |
| Water | 94 | 270 | 0.032 | 34 | 12.4 | 2.8 | 45% |
| Water | 110 | 410 | 0.041 | 38 | 12.3 | 3.9 | 51% |
| Water | 120 | 410 | 0.055 | 44 | 12.2 | 3.3 | 60% |
| Water | 80 | 550 | 0.024 | 29 | 12.1 | 6.7 | 40% |
| Water | 130 | 550 | 0.057 | 45 | 12.4 | 4.4 | 60% |
| Water | 76 | 700 | 0.020 | 27 | 11.8 | 9.3 | 38% |
| Water | 77 | 700 | 0.021 | 27 | 10.5 | 9.1 | 43% |
| Water | 140 | 130 | 0.070 | 50 | 17.0 | 0.9 | 49% |
| Water | 100 | 130 | 0.037 | 36 | 18.3 | 1.3 | 33% |
| Water | 110 | 270 | 0.040 | 38 | 18.6 | 2.5 | 33% |
| Water | 160 | 270 | 0.094 | 58 | 17.9 | 1.7 | 54% |
| Water | 140 | 420 | 0.074 | 51 | 18.0 | 2.9 | 47% |
| Water | 190 | 410 | 0.124 | 67 | 19.0 | 2.2 | 58% |
| Water | 90 | 550 | 0.029 | 32 | 17.6 | 6.2 | 30% |
| Water | 98 | 540 | 0.034 | 35 | 18.1 | 5.6 | 32% |
| Water | 150 | 560 | 0.079 | 53 | 18.7 | 3.7 | 47% |
| Water | 30 | 720 | 0.003 | 11 | 17.4 | 24 | 10% |
| Water | 60 | 700 | 0.013 | 22 | 17.9 | 12 | 20% |
| Water | 170 | 130 | 0.100 | 60 | 24.5 | 0.8 | 40% |
| Water | 82 | 130 | 0.024 | 29 | 24.4 | 1.6 | 20% |
| Water | 150 | 270 | 0.085 | 55 | 24.8 | 1.7 | 37% |
| Water | 180 | 410 | 0.120 | 65 | 25.3 | 2.2 | 43% |
| Water | 210 | 410 | 0.163 | 76 | 24.4 | 1.9 | 52% |
| Water | 160 | 550 | 0.096 | 59 | 24.6 | 3.4 | 39% |
| Water | 210 | 550 | 0.161 | 76 | 25.4 | 2.6 | 49% |
| Water | 160 | 710 | 0.093 | 58 | 23.1 | 4.4 | 41% |
| Water | 180 | 710 | 0.116 | 64 | 23.1 | 3.9 | 46% |
| 4 cP Gly | 4 | 420 | 0.001 | 20 | 8.2 | 113 | 39% |
| 4 cP Gly | 10 | 410 | 0.006 | 56 | 12.3 | 39 | 73% |
| 4 cP Gly | 14 | 130 | 0.011 | 78 | 19.5 | 9.0 | 64% |
| 4 cP Gly | 14 | 130 | 0.011 | 77 | 19.3 | 9.1 | 64% |
| 4 cP Gly | 13 | 270 | 0.009 | 70 | 19.5 | 20 | 58% |
| 4 cP Gly | 17 | 410 | 0.016 | 92 | 18.1 | 24 | 81% |

| Liquid [a] | $Re_{LS}$ | $Re_{GS}$ | $We_{LS}$ | Ca ($x10^5$) | $\Delta P$ [b] (in. WC) | $Re_{GS}/Re_{LS}$ | $Q_{max}/Q_{pt}$ [c] |
|---|---|---|---|---|---|---|---|
| 4 cP Gly | 10 | 550 | 0.006 | 54 | 20.6 | 55 | 42% |
| 4 cP Gly | 11 | 700 | 0.007 | 61 | 19.0 | 62 | 52% |
| 4 cP Gly | 17 | 410 | 0.016 | 93 | 24.4 | 24 | 61% |
| 4 cP Gly | 18 | 410 | 0.018 | 99 | 26.4 | 22 | 61% |
| 14 cP Gly | 0.4 | 410 | 0.00012 | 27 | 7.5 | 910 | 54% |
| 14 cP Gly | 1.2 | 400 | 0.00080 | 69 | 14.4 | 340 | 73% |
| 14 cP Gly | 2.0 | 130 | 0.00226 | 115 | 20.0 | 66 | 88% |
| 14 cP Gly | 1.9 | 260 | 0.00217 | 113 | 21.0 | 140 | 82% |
| 14 cP Gly | 2.0 | 410 | 0.00236 | 118 | 20.5 | 203 | 88% |
| 14 cP Gly | 1.9 | 530 | 0.00205 | 110 | 21.0 | 280 | 80% |
| 14 cP Gly | 1.2 | 700 | 0.00088 | 72 | 18.5 | 570 | 60% |
| 14 cP Gly | 2.0 | 400 | 0.00230 | 117 | 26.3 | 204 | 68% |
| Decane | 200 | 130 | 0.42746 | 75 | 18.8 | 0.7 | 61% |
| Decane | 220 | 400 | 0.52012 | 83 | 19.6 | 1.9 | 65% |
| Decane | 150 | 400 | 0.25484 | 58 | 9.9 | 2.7 | 90% |

[a] Physical properties and dimensionless groups for the liquids that were tested are shown in Table A.2.
[b] The pressure difference across the pore throat at the break through point.
[c] Calculated maximum flow of liquid without breakthrough of liquid to the gas outlet divided by the maximum flow capacity of the pore throat at the given $\Delta P$.

**Table A.2. Physical properties and dimensionless groups characterizing the liquids tested.**

| Liquid | Density (g/cc) | Viscosity (cP) | Surface Tension (Dyne/cm) | $\mu_L/\mu_G$ | Bo | Su ($x10^{-3}$) |
|---|---|---|---|---|---|---|
| Water | 1.0 | 1 | 72 | 60 | 2.8 | 280 |
| 4 cP Gly | 1.09 | 4 | 70 | 240 | 3.1 | 19 |
| 14 cP Gly | 1.15 | 14 | 67 | 800 | 3.5 | 1.7 |
| Decane | 0.73 | 0.9 | 23 | 50 | 6.4 | 90 |

# REPORT DOCUMENTATION PAGE

*Form Approved*
*OMB No. 0704-0188*



| 1. AGENCY USE ONLY (*Leave blank*) | 2. REPORT DATE | 3. REPORT TYPE AND DATES COVERED |
|---|---|---|
| | June 2001 | Final Contractor Report |

**4. TITLE AND SUBTITLE**

Normal Gravity Testing of a Microchannel Phase Separator for Insitu Resource Utilization

**5. FUNDING NUMBERS**

WU–101–13–0B–00
NAS3–00137

**6. AUTHOR(S)**

Ward E. TeGrotenhuis and Victoria S. Stenkamp

**7. PERFORMING ORGANIZATION NAME(S) AND ADDRESS(ES)**

Battelle Memorial Institute, Pacific Northwest Division
P.O. Box 999, 3200 Q Avenue
Richland, Washington 99352

**8. PERFORMING ORGANIZATION REPORT NUMBER**

E–12809

**9. SPONSORING/MONITORING AGENCY NAME(S) AND ADDRESS(ES)**

National Aeronautics and Space Administration
Washington, DC 20546–0001

**10. SPONSORING/MONITORING AGENCY REPORT NUMBER**

NASA CR—2001-210955

**11. SUPPLEMENTARY NOTES**

Final Report for the contract period of September 2000 to January 2001. Project Manager, John McQuillen, Microgravity Science Division, NASA Glenn Research Center, organization code 6712, 216–433–2876.

**12a. DISTRIBUTION/AVAILABILITY STATEMENT**

Unclassified - Unlimited
Subject Category: 34 Distribution: Nonstandard

Available electronically at http://gltrs.grc.nasa.gov/GLTRS

This publication is available from the NASA Center for AeroSpace Information, 301–621–0390.

**12b. DISTRIBUTION CODE**

**13. ABSTRACT** ***(Maximum 200 words)***

A microchannel separator, with 2.7 millimeters as the smallest dimension, was tested, and a pore throat structure captured and removed liquid from a gas-liquid stream. The microchannel device was tested in a horizontal orientation to minimize the influence of gravity at a wide range of gas and liquid flow rates ranging from 0.0005 up to 0.14 volume fraction of liquid. Four liquids were tested with air. The biggest factor affecting the throughput is the capacity of liquid flow through the pore throat, which is dictated by permeability, liquid viscosity, flow area, pore throat thickness, and pressure difference across the pore throat. Typically, complete separation of gas and liquid fractions was lost when the liquid flow rate reached about 40 to 60 percent of the pore throat capacity. However, this could occur over a range of 10 to 90 percent utilization of pore throat capacity. Breakthrough occurs in the microchannel phase separator at conditions similar to the annular to plug flow transition of two-phase microgravity pipe flow implying that operating in the proper flow regime is crucial. Analysis indicates that the Bond number did not affect performance, supporting the premise that hydrodynamic, interfacial, and capillary forces are more important than gravity. However, the relative importance of gravity is better discerned through testing under reduced gravity conditions.

**14. SUBJECT TERMS**

Two phase flow; Microgravity; Separation; Drying

**15. NUMBER OF PAGES**

24

**16. PRICE CODE**

| 17. SECURITY CLASSIFICATION OF REPORT | 18. SECURITY CLASSIFICATION OF THIS PAGE | 19. SECURITY CLASSIFICATION OF ABSTRACT | 20. LIMITATION OF ABSTRACT |
|---|---|---|---|
| Unclassified | Unclassified | Unclassified | |